JACS
JOURNAL OF THE AMERICAN CHEMICAL SOCIETY
Article
pubs.acs.org/JACS

Intrinsic "Vacancy Point Defect" Induced Electrochemiluminescence from Coreless Supertetrahedral Chalcogenide Nanocluster

Feng Wang,[‡,§] Jian Lin,[†,§] Tingbi Zhao,[‡] Dandan Hu,[†] Tao Wu,*[,†] and Yang Liu*[,‡]

[†]College of Chemistry, Chemical Engineering and Materials Science, Soochow University, Jiangsu 215123, China

[‡]Department of Chemistry, Beijing Key Laboratory for Analytical Methods and Instrumentation, Key Laboratory of Bioorganic Phosphorus Chemistry & Chemical Biology of Ministry of Education, Tsinghua University, Beijing 100084, China

Supporting Information

ABSTRACT: A deep understanding of distinct functional differences of various defects in semiconductor materials is conducive to effectively control and rationally tune defect-induced functionalities. However, such research goals remain a substantial challenge due to great difficulties in identifying the defect types and distinguishing their own roles, especially when various defects coexist in bulk or nanoscale material. Hereby, we subtly selected a molecular-type semiconductor material as structural mode composed of supertetrahedral chalcogenide Cd−In−S nanoclusters (NCs) with intrinsic vacancy point defect at the core site and antisite point defects at the surface of supertetrahedron and successfully established the correlation of those point defects with their own electrochemiluminescence (ECL) behaviors. The multichannel ECL properties were recorded, and the corresponding reaction mechanisms were also proposed. The predominant radiation recombination path of ECL emission peak at 585 nm was significantly distinguished from asymmetrically broad PL emission with a peak at 490 nm. In addition, the ECL performance of the coreless supertetrahedral chalcogenide nanocluster can be modulated by atomically precise doping of monomanganese ion at the core vacant site. A relatively high ECL efficiency of 2.1% was also gained. Actually, this is the first investigation of ECL behavior of semiconductor materials based on supertetrahedral chalcogenide nanocluster in aqueous solution. Current research may open up a new avenue to probe the roles of various different defects with defined composition and position in the NC. The versatile and bright ECL properties of Cd−In−S NC combined with tunable ECL potential and ECL peak suggest that the new kind of NC-based ECL material may hold great promising for its potential applications in electrochemical analysis, sensing, and imaging.

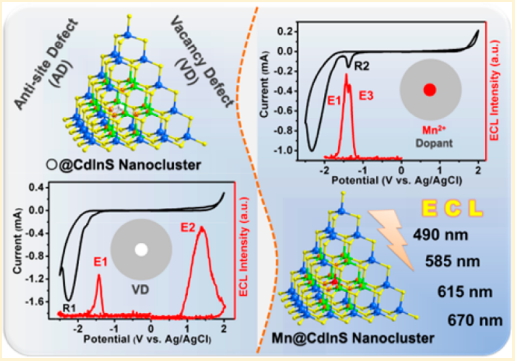

INTRODUCTION

Accurate identification and deep understanding of active sites, such as catalytic centers in molecule catalysts[1−3] or electron/hole trapping centers in solid-state semiconductor materials,[4−7] have always been the emphasis and difficulty in the research field of synthetic chemistry and material science. Compositional and structural defects in crystalline materials are generally regarded as particular active sites,[8−10] which play decisive roles in controlling and/or giving rise to a large range of electronic,[11] magnetic,[12] or optical properties.[13] However, a better understanding of the roles that various defects play on the physical or chemical properties still remains a big challenge because of great difficulties in determining the precise sites and compositions for randomly distributed and disordered defects, especially for low-dimensional point or line defects inside solid-state materials. Thus far, only various surface defects in nanoscale materials have been explored widely and thoroughly by virtue of some experimentally technological approaches, such as TEM and spherical aberration (SA)-corrected HRTEM,[14,15] which are powerless for the randomly distributed internal defects. Of note recently is an increasing interest in the exploration of ordered internal defects in some crystalline materials, such as metal−organic frameworks (MOFs)[16−18] and interrupted semiconductor zeolitic material.[19] Periodical vacancy defects in crystalline materials ensure their positions to be easily probed through single-crystal X-ray diffraction analysis. Precise position information on defects could facilitate the investigation of the influence of ordered defects on the physical or chemical properties. So far, the cases with periodically internal defects in materials are rare, especially in the important field of semiconductor materials. Creating ordered internal defects in semiconductor materials and investigating those defects-related properties will be a subject worthy of study.

Open-framework metal chalcogenides based on nanoclusters (NCs) with regular geometrical shape represent a new type of solid-state semiconductor materials with the combination of porosity and semiconducting properties.[20] In the main framework, the nanosized supertetrahedral chalcogenide NCs, being structurally precise fragments of the well-known cubic ZnS-type semiconductors, can be regarded as the smallest semiconductor NC or quantum dots (QDs). The investigation of defect chemistry for these materials has never been made before.

Received: April 9, 2016
Published: May 26, 2016

DOI: 10.1021/jacs.6b03662
J. Am. Chem. Soc. 2016, 138, 7718−7724

Recently, we reported a micrometer-sized crystal (denoted as ISC-10-EInS, E = Zn or Cd) composed of isolated coreless supertetrahedral chalcogenide NCs ($[E_6In_{28}S_{52}(SH)_4]$) with the dimension of ~2 nm in edge length (Scheme 1A).[21] The well-defined

Scheme 1. Structure of ISC-10-CdInS[a]

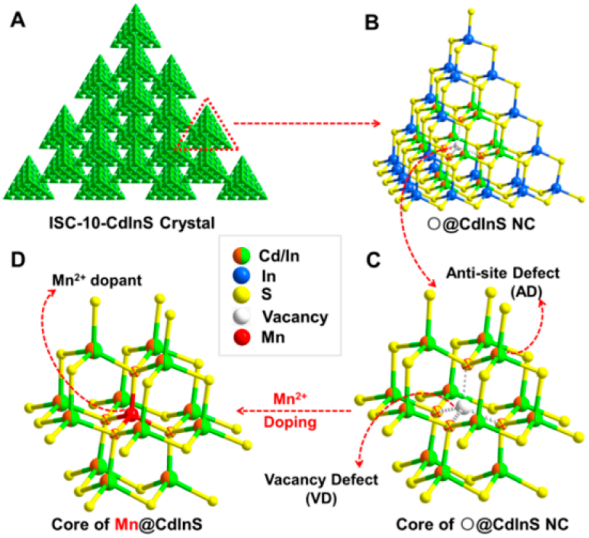

[a](A) Composed of coreless ○@CdInS NC, (B) with intrinsic internal defect and (C) anti-site defects, which can trap one Mn^{2+} dopant at its vacant core site (D).

single vacancy at the core of each supertetrahedral NC (denoted as ○@EInS, where "○" means vacancy) with 34 metal sites (6 E^{2+} ions and 28 In^{3+} ions) can be confirmed by single-crystal X-ray diffraction technique (Scheme 1B). It is worth noting that the vacant site was proved to trap a single Cu^+ or Mn^{2+} ion without the collapse of NC to form transition metal ion doped NC (denoted as M@EInS, M = Cu or Mn).[22] On the basis of the fact, such a vacancy in the NC can be rationally viewed as "vacancy point defect" (VD, denoted as V_M), and the resulting micrometer-sized crystal composed of isolated coreless NCs exhibits ordered "intrinsic internal defects" throughout the whole crystal lattice. Besides vacancy defects, there exist antisite defects (AD, denoted as In_E or E_{In}) in the NC because the six divalent ions (E^{2+}) in the NC are randomly located at the 6 out of 12 metal sites at four faces of supertetrahedron (Scheme 1C) according to elemental and structural analysis and Pauling electrostatic valence sum rule. Generally, the AD are commonly observed in ternary and quaternary chalcogenide semiconductor materials, for example, $CuInS_2$, in which a significant density of AD-related donor−acceptor states located in the band gap are created.[23−25] These antisite point defects can be also viewed as virtual surface defects as result of their locations at the surface of supertetrahedral NC. In addition, there still exist some real surface defects (SD) at the surface of crystals, especially when they are crushed into nanometer or micrometer-sized particles. Other types of defects, such as dislocation defects or interstitial defects, cannot be completely ruled out for a nonideal crystal, but they obviously belong to the minority compared with the main defects mentioned above based on exact structural and compositional information. Therefore, such crystalline material of ISC-10-EInS provides a good structure mode with coexistence of various well-defined defects for probing their own roles in chemical or physical properties. Unfortunately, previous photoluminescence (PL) studies on ISC-10-CdInS indicated that its emission spectrum only displays a broad and asymmetric shape peaked at 490 nm with a long tail (Figure S1). The excitation-wavelength-dependent emission behavior has been tentatively attributed to some complicated radiative recombination of charge carriers at some energy states induced by various defect centers. The role of point defects mentioned above cannot be exclusively distinguished through PL measurement because there are no multiple peaks to be obviously observed. Therefore, how to further establish the distinct role of these point defects in the NC and directly observe the relationship between defect structure and optical activity becomes an interesting topic and key challenge in the research field of semiconductor NCs.

Electrochemiluminescence (ECL) is a light-emission phenomenon produced by an energetic electron transfer chemical reaction between the electrochemically generated species.[26−28] Quests for new and stable ECL emitters with high efficiency and deep investigations on the relationships between the structure and ECL properties are an active and continuous theme in the realm of ECL. In fact, various kinds of semiconductor nanocrystals, or quantum dots, such as CdS,[29] CdSe,[30] CdTe,[31] PbS,[32] and ZnSe,[33] have been chosen as promising ECL emitters to actively study their bioanalytical applications such as biomedicine and bioimaging. Those studies demonstrated substantially that ECL of QDs is intrinsically sensitive to surface chemistry and surface states, which make it a very powerful tool to study surface energy states created by surface defects. Generally speaking, surface vacancies can provide localized surface states within the band gap. Thus far, ECL is mainly generated at surface states,[29,30,34−36] except a few reports that ECL can be generated at band edges.[31,37] Recently, an increasing number of reports about the effect of surface ligand,[31] nonpassivated or passivated surface atoms,[37,38] and surface charge[33] on the properties of ECL have been exploited. However, there are no reports about the effect of intrinsic internal defects on the ECL properties of QDs. Can the ordered intrinsic vacancy point defect in coreless ○@CdInS NC introduce a new energy state within the band gap to induce the ECL? Can the ECL measurement distinguish the roles of various defects with distinct energy level in the coreless ○@CdInS NC?

Herein, we for the first time successfully distinguished the active roles of point defects in semiconductor NC by virtue of ECL technology. The coreless ○@CdInS NC exhibited excellent multichannel ECL behavior with high ECL emission intensity in an aqueous solution as the result of highly efficient electron−hole recombination facilitated by point defects in the NC. A main ECL emission peak obviously observed at around 585 nm is ascribed to the contribution of the vacancy defect. A similar result was also observed in ○@ZnInS NC with a similar type of point defects. In addition, compared with that observed in ○@CdInS NC, Mn^{2+} dopant locating at the vacant site of NC (Mn@CdInS) induced a new main ECL emission peak with a red-shifted emission wavelength (615 nm) at lower cathode potential by introducing some new intermediate electronic states. Current results reveal that supertetrahedral chalcogenide NC-based semiconductor materials with intrinsic defects could serve as some promising ECL emitters in the application of bioimaging and sensing.

EXPERIMENTAL SECTION

Chemicals and Materials. Sodium sulfite, potassium persulfate ($K_2S_2O_8$, 99.5%), and tripropylamine (TPrA, 98%) were purchased from three chemical reagent factory of Tianjin. Hydrogen peroxide (H_2O_2), superoxide dismutase (SOD), sodium phosphate monobasic

DOI: 10.1021/jacs.6b03662
J. Am. Chem. Soc. 2016, 138, 7718−7724

dehydrate ($NaH_2PO_4·2H_2O$, AR, 99%), sodium phosphate dibasic dodecahydrate ($Na_2HPO_4·12H_2O$, AR, 99%), cadmium nitrate tetrahydrate ($Cd(NO_3)_2·4H_2O$, AR, 99%), zinc nitrate hexahydrate ($Zn(NO_3)_2·6H_2O$, AR, 99%), indium powder (In, 99.99%, 200 mesh), sulfur power (S, 99.99% metal basis), manganese(II) acetate tetrahydrate ($Mn(Ac)_2·4H_2O$, 99.99% metal basis), piperidine (PR, 99%), and 1,5-diazabicyclo[4.3.0]non-5-ene (DBN, 98%) were purchased from Aladdin Industrial, Inc. All chemicals were used as received without further purification.

Syntheses. The nanometer- and micrometer-sized crystals of ISC-10-CdInS, ISC-10-ZnInS, and corresponding Mn-doped samples were synthesized by literature methods.[22]

Immobilization of NC on Glassy Carbon Electrode. ○@CdInS, ○@ZnInS, and Mn@CdInS aqueous suspensions (0.2 mg/mL) were obtained by dispersing corresponding resultants into water under ultrasonication for at least 1 h and were used as samples to test properties of electrochemical and ECL. Glassy carbon electrodes (GCE) with diameter of 3 mm were polished and ultrasonically cleaned in ethanol and water subsequently before use. Then, 10 μL of sample suspension was dropped on the surface of GCE and dried in the dark at room temperature.

PL, Electrochemical, and ECL Measurements. The PL spectra were recorded via an Edinburgh FLS-920 steady state and time-resolved fluorescence spectrophotometer equipped with a 450 W xenon lamp. The ECL and electrochemical measurements conducted in a three-electrode electrochemical system with a GCE working electrode, a Pt-wire counter electrode, and Ag/AgCl reference electrode were carried out on an ECL detection system (MPI-B, Remex Electronic Instrument Ltd. Co. Xi'an, China). The photomultiplier tube (PMT) was biased at 750 V, the amplifier series was held at 3, and the scan rate was held at 0.1 V/s, unless otherwise specified. The ECL spectra were measured by collecting the various ECL intensities based on typical cyclic voltammetry with band-pass filters at the wavelengths of 440, 460, 490, 535, 555, 575, 620, 640, 680, 705, and 745 nm used in the detection system; afterward, the difference of the ECL intensity was plotted with the corresponding wavelength. The PMT was biased at 1000 V, the amplifier series was held at 4, and the scan rate was 0.5 V/s, unless otherwise specified.

RESULTS AND DISCUSSION

Electrochemical and ECL Behaviors of ○@CdInS NC Modified GCE. Figure 1A shows a typical cyclic voltammetric (CV) curve of ○@CdInS NC modified GCE in phosphate buffer solution (PBS) bubbled with N_2 for 25 min. In the CV curve, there is one obvious reduction peak (assigned as R1) in the cathodic region with half-wave potential of −2.015 V. To study the origin of the R1, the ○@CdInS NC modified GCE was incubated in $InCl_3$ solution and Na_2S solution, respectively, and the CV curves were recorded (Figure S2). It is observed that R1 still exists after soaking in both Na_2S solution and $InCl_3$ solution, respectively. In addition, the CV curves of the electrodes coated with organic amine molecules, i.e. 1, 5-diazabicyclo[4.3.0]non-5-ene (DBN) and piperidine (PR) serving as counterions in the crystal lattice of ISC-10-EInS, present no redox peaks in the potential region (Figure S3). As mentioned in the Introduction, the well-defined vacant sites at the core of coreless ○@CdInS NC can be treated as ideal intrinsic internal defects, which prefer trapping a transition metal ion (Mn^{2+} or Cu^{+}). Therefore, such a vacancy defect could introduce an energy state as hole acceptor being close to and above valence band (VB). On the basis of above results and analyses, R1 reduction peak mainly resulted from the electron injection into AD-induced energy state and conduction band (CB) in the NCs, instead being caused by the reduction reaction of compositions in the selected semiconductor material.

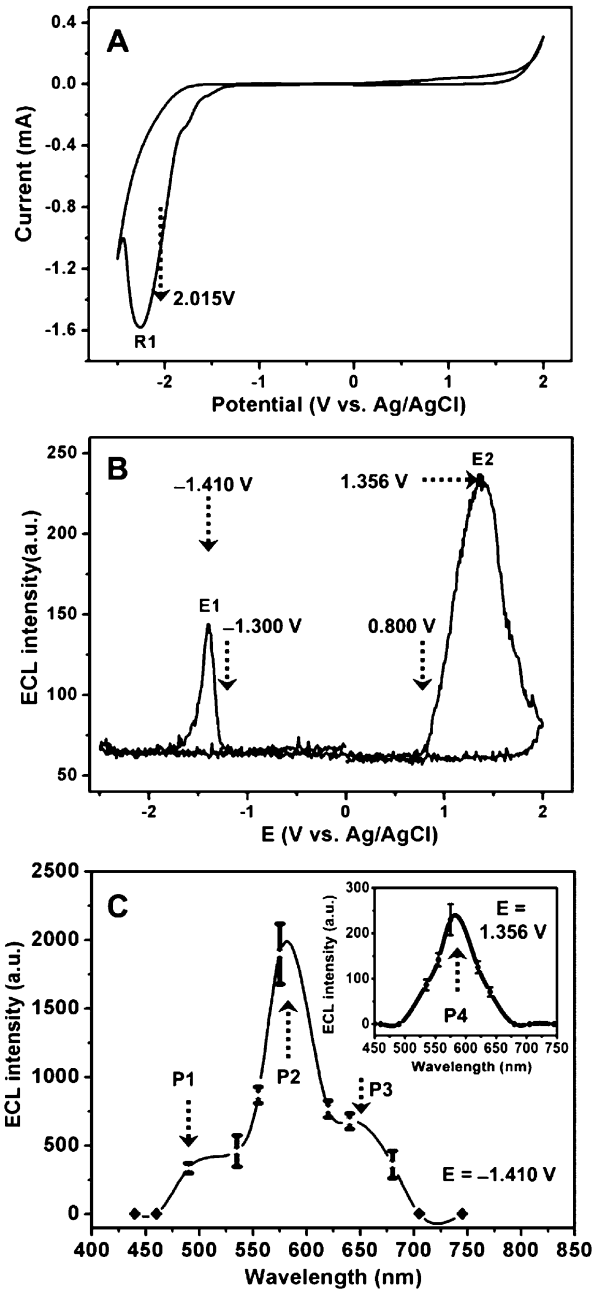

Figure 1. (A) CV curve of the ○@CdInS NC modified GCE in 0.1 M PBS bubbled with N_2 for 25 min. (B) ECL potential curve of the ○@CdInS NC modified GCE in 0.1 M PBS bubbled with N_2 for 25 min. (C) ECL spectrum of ○@CdInS NC modified GCE in PBS at −1.410 V, corresponding to E1 emission in B. Inset represents ECL spectrum at 1.356 V, corresponding to E2 emission in B.

Figure 1B shows the ECL potential curve for ○@CdInS NC modified GCE in PBS bubbled with N_2 for 25 min. In the cathodic region, there is a sharp ECL emission peak (assigned as E1) which starts from −1.300 V with a peak at −1.410 V. In the anodic region, the strong ECL emission peak (assigned as E2) starts from 0.800 V and is centered at 1.356 V. The potential gap between the onset potential of E1 (−1.300 V) and E2 (0.800 V) is calculated to be 2.100 eV, which is theoretically equal to a light emission with the wavelength of 590 nm. Considering the large potential gap between R1 and E1, E1 should be related to defects in the ○@CdInS NC. To further

DOI: 10.1021/jacs.6b03662
J. Am. Chem. Soc. 2016, 138, 7718−7724

investigate the radiative recombination path of E1 emission, ECL spectrum of E1 emission was also studied, as shown in Figure 1C. A main ECL emission peak (P2) is obviously observed at around 585 nm. In addition, two weak shoulder peaks (P1 and P3) are also observed. The P1 peak at around 490 nm is very similar to that observed in PL spectrum of ○@CdInS NC. Apparently, the strong ECL emission peak (P2) at 585 nm cannot be observed in its PL spectrum. E1 peak can be observed by the negative one-way scanning so that is not the annihilation mechanism but must be dependent on the oxidized species as coreactant in the electrolyte. As shown in Figure S4, the E1 emission can be significantly suppressed by the addition of superoxide dismutase (removing superoxide radical) or the injection of N_2. When dissolved oxygen was further removed by adding Na_2SO_3 to the electrolyte,[38] E1 disappeared. Moreover, E1 emission intensity can be increased by the addition of H_2O_2 or the injection of O_2. All of these results suggest that dissolved oxygen in the electrolyte is the coreactant. In addition, E2 exhibits one ECL emission peak (P4) at around 585 nm (inset of Figure 1C), similar to the P2 peak in E1 emission. This result demonstrates the same radiative recombination pathway for P2 peak in E1 emission and P4 peak in E2 emission. It is noteworthy that E2 emission at positive scanning can only be obtained by the negative scan first. In addition, E1 and E2 emission can be also observed in the GCE modified by ○@ZnInS NC with the same intrinsic internal defect structure (Figure S5).

Previous studies have revealed that PL emission at 490 nm is attributed to radiative recombination of charge carriers at AD-induced trap state (ATS), which are close to CB and VB of NC.[22] Therefore, it is quite reasonable to ascribe P1 peak in E1 emission as radiative recombination of charge carriers at ATS, similar to the electron−hole pair recombination mechanism occurred in PL process. As shown in Scheme 2a, during negative scan, the electrode directly injects electrons at ATS below CB in NC, and the oxidizing coreactant (O_2 or H_2O_2) simultaneously creates a hole at VB of NC, which quickly diffuses to ATS above VB. Before reasonably identifying the origin of P2 peak, two basic facts should be concerned. The first one is that P2 peak in E1 emission has the same wavelength value (585 nm) with P4 peak in E2 emission, both of which are coincidently very close to 590 nm calculated from the potential gap between the onset potential of E1 and E2. The other one is that E2 emission can only be obtained by the necessary negative scanning followed by subsequent positive scanning, which means that negatively charged NC (denoted as $(NC)_{ATS}^{-\bullet}$) with the injected electron at ATS below CB from cathode is very stable. Theoretically, the intrinsic vacancy defect at the core of NC could introduce an energy trap state (VTS) above VB serving as hole acceptor. With the help of the oxidative coreactant or during positive scanning, a hole will be introduced at VTS to form a positively charged NC (denoted as $(NC)_{VTS}^{+\bullet}$). On the basis of the above facts and theoretical analysis, P2 peak at 585 nm may be tentatively attributed to the recombination of the electron on ATS below CB and the hole on VTS above VB. The energy level at VTS is even higher than that of ATS above VB because of the shorter emission wavelength of P2 relative to that of P1 peak.[22] To clearly describe the origin of emission peaks in E1 and E2, the energy band structure and ECL radiations can be represented as shown in Scheme 2. According to the configuration, the possible mechanism of P2 peak during cathodic scanning is proposed as follows:

$$O_2 + 2H_2O + 2e^- \rightarrow H_2O_2 + 2OH^- \quad (1)$$

Scheme 2. Energy Band Structure of NC and ECL Radiation Paths[a]

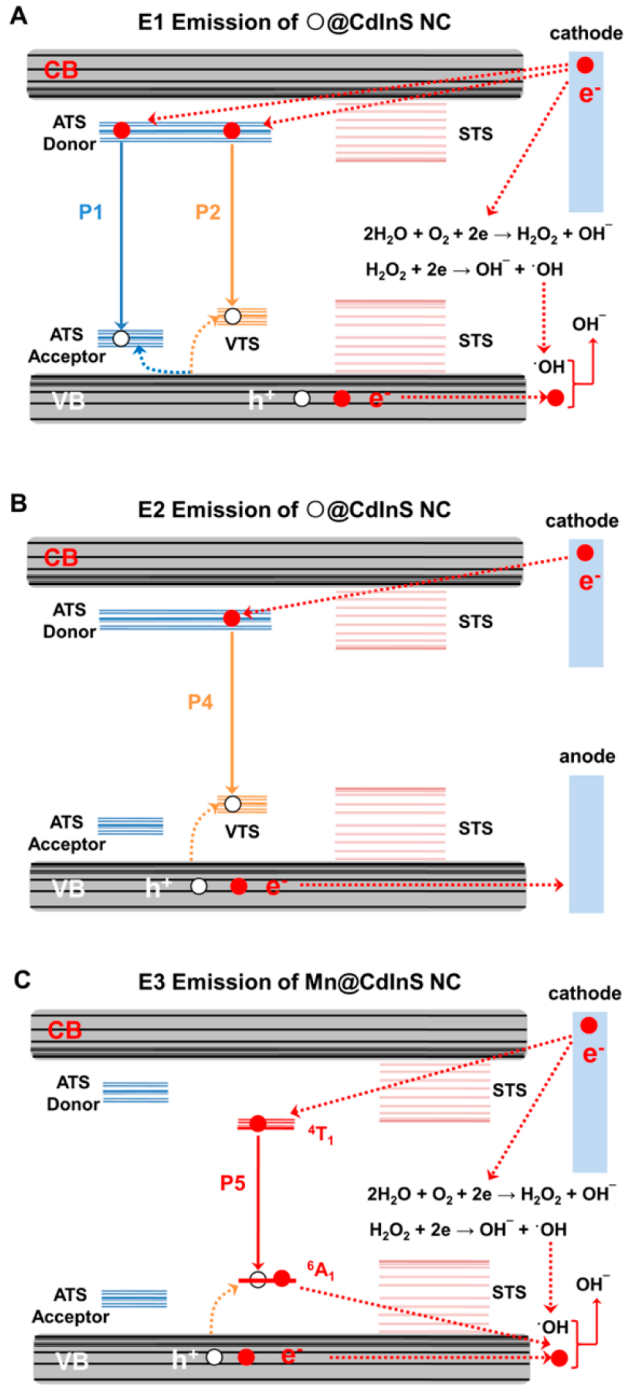

[a](A) E1 and (B) E2 emission of ○@CdInS NC; (C) E3 emission of Mn@CdInS NC.

$$H_2O_2 + e^- \rightarrow OH^- + {}^{\bullet}OH \quad (2)$$

$$NC + {}^{\bullet}OH \rightarrow (NC)_{VTS}^{+\bullet} + OH^- \quad (3)$$

$$(NC)_{VTS}^{+\bullet} + e^- \rightarrow (NC)_{ATS\text{-}VTS}^{*} \quad (4)$$

$$(NC)_{ATS\text{-}VTS}^{*} \rightarrow NC + h\nu \quad (5)$$

During negative scanning in the presence of coreactant, the oxidizing coreactant ($^{\bullet}OH$) can directly get rid of one electron

DOI: 10.1021/jacs.6b03662
J. Am. Chem. Soc. 2016, 138, 7718−7724

at VTS from NC and introduce a hole at VTS to form $(NC)_{ATS}^{+\bullet}$ species (eq 3). Of course, the oxidizing coreactant ($^{\bullet}OH$) can also inject a hole at VB, which then quickly diffuses to VTS. With further negative scanning, the electron is directly injected to ATS below CB in $(NC)_{ATS}^{+\bullet}$ species to form an excited NC (denoted as $(NC)_{ATS\text{-}VTS}^{*}$, eq 4). Finally, P2 peak at 585 nm is obtained when the excited NC de-excites to the ground state (eq 5), as shown in Scheme 2A. Different from P2 peak, P4 peak is originated from an annihilation mechanism of redox species of ○@CdInS NC itself. The possible mechanism of P4 emission is proposed as follows.

$$NC + e^{-} \rightarrow (NC)_{ATS}^{-\bullet} \quad (6)$$

$$NC \rightarrow (NC)_{VTS}^{+\bullet} + e^{-} \quad (7)$$

$$(NC)_{ATS}^{-\bullet} + (NC)_{VTS}^{+\bullet} \rightarrow (NC)_{ATS\text{-}VTS}^{*} + NC \quad (8)$$

$$(NC)_{ATS\text{-}VTS}^{*} \rightarrow NC + h\nu \quad (9)$$

The negatively charged $(NC)_{ATS}^{-\bullet}$ species (eq 6) and positively charged $(NC)_{VTS}^{+\bullet}$ species (eq 7) are produced by the successive cathodic and anodic scans. The two charged NCs annihilate each other to form the excited $(NC)_{ATS\text{-}VTS}^{*}$, which finally emits P4 peak at 585 nm in the de-excitation process (Scheme 2B). The intensity of anodic E2 emission is much greater than that of cathodic E1 emission, indicating that $(NC)_{ATS}^{-\bullet}$ species is more stable than $(NC)_{VTS}^{+\bullet}$. This could be explained by the reason that the holes are more preferably trapped on VTS than ATS or STS during positive scanning.

ECL Property of Mn@CdInS NC. Figure 2 shows the CV curve and the ECL potential curve of Mn@CdInS NC modified GCE in PBS bubbled with N_2 for 25 min. Besides the peak at the similar potential with R1 originated from the electron injection into the NCs, there is a new reduction peak with half-wave potential of −1.315 V (assigned as R2) in the CV curve of Mn@CdInS NC (Figure 2A). Considering the intrinsic differences in composition between Mn@CdInS and ○@CdInS NC, R2 peak can only be ascribed to the doped Mn^{2+} ion in Mn@CdInS NC. A new ECL emission (assigned as E3) was also observed at the same potential of R2 (Figure 2B). To further demonstrate the mechanism of E3 emission, the ECL spectrum of E3 was studied as shown in Figure 2C. The main ECL emission spectrum with a peak (P5) at 615 nm is similar to the PL spectrum (630 nm) of Mn@CdInS NC (Figure S1) when the coarse wavelength interval (20 nm) of the band-pass filters used in the spectrum measurement is taken into consideration.

As previously reported, Mn^{2+} dopant at the core of Mn@CdInS NC introduces a new trap state within the band gap of ○@CdInS NC. According to the Tanabe−Sugano diagrams, the lowest excited state (^4G) of free Mn^{2+} ion will split into four energy levels ($^4T_1$, $^4T_2$, ^4E, and $^4A_1$).[39] As a result, the corresponding energy band structure and ECL radiations can be represented as shown in Scheme 2C. E3 emission comes from the radiative recombination between the energy states of $^4T_1$ and $^6A_1$ within the Mn^{2+} ion. The intensity of ECL emission was reduced after injecting N_2 to the solution (Figure S6). This indicates that the dissolved oxygen is also most likely to act as electron acceptor to take part in E3 ECL emission. Thus, the possible mechanism of E3 emission is proposed as follows:

$$O_2 + 2H_2O + 2e^{-} \rightarrow H_2O_2 + 2OH^{-} \quad (10)$$

$$H_2O_2 + e^{-} \rightarrow OH^{-} + {}^{\bullet}OH \quad (11)$$

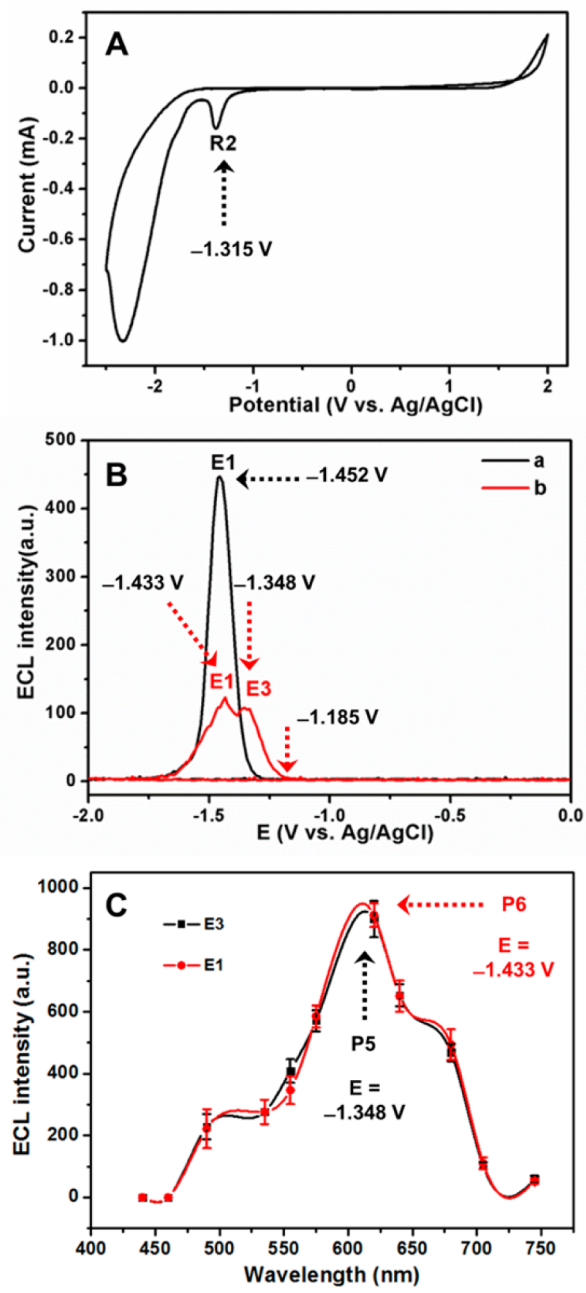

Figure 2. (A) CV curve of Mn@CdInS NC modified GCE in 0.1 M PBS bubbled with N_2 for 25 min. (B) ECL-potential curve of ○@CdInS (a) and Mn@CdInS (b) NC modified GCE in 0.1 M PBS when the electrode potential was scanned from 0 to −2.2 V in 0.1 M PBS. (C) ECL spectra of Mn@CdInS NC modified GCE at −1.348 V (a) and −1.433 V (b), corresponding to E3 and E1 emission in B, respectively.

$$Mn^{2+} + {}^{\bullet}OH \rightarrow Mn^{3+} + OH^{-} \quad (12)$$

$$Mn^{3+} + e^{-} \rightarrow (Mn^{2+})^{*} \quad (13)$$

$$(Mn^{2+})^{*} \rightarrow Mn^{2+} + h\nu \quad (14)$$

In eq 12, the formed oxidative $^{\bullet}OH$ radical easily injects a hole into the Mn^{2+} to form Mn^{3+}, which subsequently recombines with trapped electron from cathode to result in the formation of an excited state of $(Mn^{2+})^{*}$ (eq 13). When the Mn^{2+} returns from the excited state to ground state, light is emitted. In this case, R2 peak in the CV curve can be explained by the

DOI: 10.1021/jacs.6b03662
J. Am. Chem. Soc. 2016, 138, 7718−7724

electro-reduction of Mn^{3+} to form $(Mn^{2+})^*$ during the negative scanning.[40,41]

It is notable that as for E1 emission of Mn@CdInS NC (Figure 2C) there is a main ECL peak (P6) at 615 nm, which is similar to P5 peak from E3 emission and has a dramatic redshift relative to that of P2 peak (585 nm) in E1 emission from ○@CdInS NC. This indicates that the electrons on ATS injected by electrode can easily transfer to $^4T_1$ state of Mn^{2+}, and subsequent recombination with holes on $^6A_1$ state of Mn^{2+} injected by $^{\bullet}OH$ radical gives rise to ECL emission (Scheme S1). These facts also demonstrate that a precisely doped Mn^{2+} ion not only results in a new red emission peak for the doped NC but also markedly suppresses intrinsic P2 peak observed in undoped ○@CdInS NC during negative scanning.

ECL Efficiency of ○@CdInS and Mn@CdInS NC. The ECL efficiency of different systems was calculated verus that of $[Ru(bpy)_3]^{2+}$/solution system, which is shown in Table 1.

Table 1. ECL Efficiencies of Modified Films Compared to Solution-Phase $[Ru(bpy)_3]^{2+}$

material	ECL efficiency	PBS (%)	$K_2S_2O_8$ (%)	TPrA (%)
○@CdInS film	cathodic	0.66	0.13	
	anodic	0.045		2.1
Mn@CdInS film	cathodic	0.0085[a]	0.036	
	anodic	0.095		0.8

[a]ECL efficiency of Mn@CdInS was calculated on the basis of E3.

The quantum efficiency for ECL is defined as the number of photons per electron transferred. The relative ECL efficiency was calculated using the relation below:[42]

$$\Phi_x = \Phi_{st}\left(\frac{\int_0^t I\,dt}{\int_0^t i\,dt}\right)_x \Big/ \left(\frac{\int_0^t I\,dt}{\int_0^t i\,dt}\right)_{st}$$

$$= \Phi_{st}\left(\frac{\int_a^b I\,dv}{\int_a^b i\,dv}\right)_x \Big/ \left(\frac{\int_a^b I\,dv}{\int_a^b i\,dv}\right)_{st}$$

Here, Φ_{st} is the ECL efficiency of $[Ru(bpy)_3]^{2+}$/(1 mM and 0.1 M (TBA)BF_4/ACN) via annihilation, taken as 5.0%, I is ECL intensity, i^0 is current value, and x is the sample. Because $[Ru(bpy)_3]^{2+}$ itself cannot form a film, 100 uM $[Ru(bpy)_3]^{2+}$ in solution was selected as the standard (st) of the calculation of the overall ECL efficiency for the thin film.[43]

For cathodic ECL emission in PBS bubbled with N_2 for 25 min, ○@CdInS NC has a higher ECL efficiency comparable with that of Mn@CdInS NC. The facts indicate that existence of vacancy defects is the cause of ECL emission for ○@CdInS, and the higher ECL efficiency, the more vacancy defects. Among all the above cases, the ○@CdInS/TPrA system has the highest ECL efficiency of 2.1%. To evaluate the ECL efficiency of ○@CdInS/TPrA, the ECL efficiency of ○@CdInS/TPrA was compared with that of some modified films[43,44] or single crystal,[45] as shown in Table 2. Obviously, the ECL efficiency of ○@CdInS/TPrA is relatively high, which suggests that ○@CdInS NC could be an excellent and promising candidate for ECL emitter and sensing.

CONCLUSIONS

The ECL properties of a NC-based crystalline semiconductor material composed of Cd−In−S supertetrahedral chalcogenide NC with intrinsic vacancy point defect has been investigated for the first time. The correlation of various defects with their own ECL behaviors was established, and the corresponding possible ECL mechanisms were also proposed. It is notably that the ECL emission peak at 585 nm is exclusively associated with an internal vacancy defect in the NC, which is clearly distinguished from that of the antisite defect. Furthermore, atomically precise doping of mono manganese ion at a vacant site of NC can give rise to a Mn^{2+}-related ECL emission peak (615 nm) under the lower cathode potential and suppress ECL emission related with vacancy defect. A relatively high ECL efficiency of 2.1% was gained. This preliminary work elucidates that intrinsic internal defects in NC could get involved to induce desirable ECL behavior, extends the application of ECL technology in probing the internal defect structure in NC, and promotes a new kind of NC-based ECL emitter which may hold great promise for applications in sensing and imaging. In addition, the effect of other transition metal ions on ECL performances of Cd−In−S NC will form the subject of future studies.

Table 2. Comparison of ECL Efficiencies for Different ECL Systems

material (environment)[a]	Φ_{ECL} (%)	ref
Nafion-$[Ru(bpy)_3]^{2+}$ ($Na_2C_2O_4$)	0.089	46
$[Ru(Bpy)_2(PVP)_{10}]^{2+}$ ($Na_2C_2O_4$)	0.152	
Mn-doped ZnS (persulfate)	0.3	45
single-crystal ZnS (persulfate)	0.2	
○@CdInS (TPrA)	2.1	this work
Mn@CdInS (TPrA)	0.8	

[a]Bpy =2, 2′-bipyridine; PVP = polyvinylpyrrolidone.

ASSOCIATED CONTENT

Supporting Information

The Supporting Information is available free of charge on the ACS Publications website at DOI: 10.1021/jacs.6b03662.

Additional figures on PL spectra, CV curves, and ECL spectra (PDF)

AUTHOR INFORMATION

Corresponding Authors

*wutao@suda.edu.cn

*liu-yang@mail.tsinghua.edu.cn

Author Contributions

§F.W. and J.L. contributed equally to this work.

Notes

The authors declare no competing financial interest.

ACKNOWLEDGMENTS

This work was supported by National Natural Science Foundation of China (Nos. 21271135, 21375073, and 21235004), Tsinghua University Initiative Scientific Research Program (2014z21027), a start-up fund (Q410900712) from Soochow University, the Priority Academic Program Development of Jiangsu Higher Education Institutions (PAPD), and the Young Thousand Talented program, and a graduate student fund (KYZZ15_0323) from Scientific Research Innovation Projects of Jiangsu Province.

REFERENCES

(1) Karunadasa, H. I.; Montalvo, E.; Sun, Y. J.; Majda, M.; Long, J. R.; Chang, C. J. *Science* **2012**, 335, 698.

DOI: 10.1021/jacs.6b03662
J. Am. Chem. Soc. 2016, 138, 7718−7724

(2) Amakawa, K.; Wrabetz, S.; Krohnert, J.; Tzolova-Muller, G.; Schlogl, R.; Trunschke, A. *J. Am. Chem. Soc.* **2012**, *134*, 11462.
(3) McInnis, J. P.; Delferro, M.; Marks, T. J. *Acc. Chem. Res.* **2014**, *47*, 2545.
(4) Dou, L. T.; Wong, A. B.; Yu, Y.; Lai, M. L.; Kornienko, N.; Eaton, S. W.; Fu, A.; Bischak, C. G.; Ma, J.; Ding, T. N.; Ginsberg, N. S.; Wang, L. W.; Alivisatos, A. P.; Yang, P. D. *Science* **2015**, *349*, 1518.
(5) Liu, B.; Chen, H. M.; Liu, C.; Andrews, S. C.; Hahn, C.; Yang, P. D. *J. Am. Chem. Soc.* **2013**, *135*, 9995.
(6) Youngblood, W. J.; Lee, S. H. A.; Maeda, K.; Mallouk, T. E. *Acc. Chem. Res.* **2009**, *42*, 1966.
(7) Zhao, Y. X.; Vargas-Barbosa, N. M.; Strayer, M. E.; McCool, N. S.; Pandelia, M. E.; Saunders, T. P.; Swierk, J. R.; Callejas, J. F.; Jensen, L.; Mallouk, T. E. *J. Am. Chem. Soc.* **2015**, *137*, 8749.
(8) Ulvestad, A.; Singer, A.; Clark, J. N.; Cho, H. M.; Kim, J. W.; Harder, R.; Maser, J.; Meng, Y. S.; Shpyrko, O. G. *Science* **2015**, *348*, 1344.
(9) Wendt, S.; Sprunger, P. T.; Lira, E.; Madsen, G. K. H.; Li, Z. S.; Hansen, J. O.; Matthiesen, J.; Blekinge-Rasmussen, A.; Laegsgaard, E.; Hammer, B.; Besenbacher, F. *Science* **2008**, *320*, 1755.
(10) Dogan, F.; Long, B. R.; Croy, J. R.; Gallagher, K. G.; Iddir, H.; Russell, J. T.; Balasubramanian, M.; Key, B. *J. Am. Chem. Soc.* **2015**, *137*, 2328.
(11) Meng, W.; Saparov, B.; Hong, F.; Wang, J.; Mitzi, D. B.; Yan, Y. *Chem. Mater.* **2016**, *28*, 821.
(12) Sturza, M.; Allred, J. M.; Malliakas, C. D.; Bugaris, D. E.; Han, F.; Chung, D. Y.; Kanatzidis, M. G. *Chem. Mater.* **2015**, *27*, 3280.
(13) Tay, Q.; Kanhere, P.; Ng, C. F.; Chen, S.; Chakraborty, S.; Huan, A. C. H.; Sum, T. C.; Ahuja, R.; Chen, Z. *Chem. Mater.* **2015**, *27*, 4930.
(14) Janssen, Y.; Santhanagopalan, D.; Qian, D.; Chi, M.; Wang, X.; Hoffmann, C.; Meng, Y. S.; Khalifah, P. G. *Chem. Mater.* **2013**, *25*, 4574.
(15) He, S.; Li, C.; Chen, H.; Su, D.; Zhang, B.; Cao, X.; Wang, B.; Wei, M.; Evans, D. G.; Duan, X. *Chem. Mater.* **2013**, *25*, 1040.
(16) Fang, Z.; Bueken, B.; De Vos, D. E.; Fischer, R. A. *Angew. Chem., Int. Ed.* **2015**, *54*, 7234.
(17) Cliffe, M. J.; Wan, W.; Zou, X.; Chater, P. A.; Kleppe, A. K.; Tucker, M. G.; Wilhelm, H.; Funnell, N. P.; Coudert, F.-X.; Goodwin, A. L. *Nat. Commun.* **2014**, *5*, 4176.
(18) Taylor, J. M.; Komatsu, T.; Dekura, S.; Otsubo, K.; Takata, M.; Kitagawa, H. *J. Am. Chem. Soc.* **2015**, *137*, 11498.
(19) Lin, J.; Dong, Y. Z.; Zhang, Q.; Hu, D. D.; Li, N.; Wang, L.; Liu, Y.; Wu, T. *Angew. Chem., Int. Ed.* **2015**, *54*, 5103.
(20) Feng, P.; Bu, X.; Zheng, N. *Acc. Chem. Res.* **2005**, *38*, 293.
(21) Wu, T.; Zhang, Q.; Hou, Y.; Wang, L.; Mao, C.; Zheng, S.-T.; Bu, X.; Feng, P. *J. Am. Chem. Soc.* **2013**, *135*, 10250.
(22) Lin, J.; Zhang, Q.; Wang, L.; Liu, X.; Yan, W.; Wu, T.; Bu, X.; Feng, P. *J. Am. Chem. Soc.* **2014**, *136*, 4769.
(23) Aldakov, D.; Lefrancois, A.; Reiss, P. *J. Mater. Chem. C* **2013**, *1*, 3756.
(24) Castro, S. L.; Bailey, S. G.; Raffaelle, R. P.; Banger, K. K.; Hepp, A. F. *J. Phys. Chem. B* **2004**, *108*, 12429.
(25) Chen, B.; Zhong, H.; Zhang, W.; Tan, Z. a.; Li, Y.; Yu, C.; Zhai, T.; Bando, Y.; Yang, S.; Zou, B. *Adv. Funct. Mater.* **2012**, *22*, 2081.
(26) Richter, M. M. *Chem. Rev.* **2004**, *104*, 3003.
(27) Miao, W. J. *Chem. Rev.* **2008**, *108*, 2506.
(28) Wu, P.; Hou, X.; Xu, J. J.; Chen, H. Y. *Chem. Rev.* **2014**, *114*, 11027.
(29) Wang, Y.; Lu, J.; Tang, L. H.; Chang, H. X.; Li, J. H. *Anal Chem* **2009**, *81*, 9710.
(30) Myung, N.; Ding, Z. F.; Bard, A. J. *Nano Lett.* **2002**, *2*, 1315.
(31) Bae, Y.; Myung, N.; Bard, A. J. *Nano Lett.* **2004**, *4*, 1153.
(32) Hesari, M.; Swanick, K. N.; Lu, J. S.; Whyte, R.; Wang, S. N.; Ding, Z. F. *J. Am. Chem. Soc.* **2015**, *137*, 11266.
(33) Liu, S. L.; Zhang, Q. H.; Zhang, L.; Gu, L.; Zou, G. Z.; Bao, J. C.; Dai, Z. H. *J. Am. Chem. Soc.* **2016**, *138*, 1154.
(34) Ding, Z. F.; Quinn, B. M.; Haram, S. K.; Pell, L. E.; Korgel, B. A.; Bard, A. J. *Science* **2002**, *296*, 1293.
(35) Xu, S.; Liu, Y.; Wang, T.; Li, J. *Anal. Chem.* **2010**, *82*, 9566.
(36) Sun, L. F.; Bao, L.; Hyun, B. R.; Bartnik, A. C.; Zhong, Y. W.; Reed, J. C.; Pang, D. W.; Abruna, H. D.; Malliaras, G. G.; Wise, F. W. *Nano Lett.* **2009**, *9*, 789.
(37) Myung, N.; Bae, Y.; Bard, A. J. *Nano Lett.* **2003**, *3*, 1053.
(38) Fang, Y. M.; Sun, J. J.; Wu, A. H.; Su, X. L.; Chen, G. N. *Langmuir* **2009**, *25*, 555.
(39) Tanaka, M.; Qi, J.; Masumoto, Y. *J. Lumin.* **2000**, *87−89*, 472.
(40) Wang, X. F.; Xu, J. J.; Chen, H. Y. *J. Phys. Chem. C* **2008**, *112*, 17581.
(41) Suyver, J. F.; Wuister, S. F.; Kelly, J. J.; Meijerink, A. *Nano Lett.* **2001**, *1*, 429.
(42) Ouyang, J. B.; Fan, F. R. F.; Bard, A. J. *J. Electrochem. Soc.* **1989**, *136*, 1033.
(43) Wang, S. J.; Harris, E.; Shi, J. A.; Chen, A.; Parajuli, S.; Jing, X. H.; Miao, W. *Phys. Chem. Chem. Phys.* **2010**, *12*, 10073.
(44) Richter, M. M.; Debad, J. D.; Striplin, D. R.; Crosby, G. A.; Bard, A. *Anal. Chem.* **1996**, *68*, 4370.
(45) O'Reilly, E. J.; Keyes, T. E.; Forster, R. J.; Dennany, L. *Analyst* **2013**, *138*, 677.
(46) Molapo, K. M.; Venkatanarayanan, A.; Dolan, C. M.; Prendergast, U.; Baker, P. G.; Iwuoha, E. I.; Keyes, T. E.; Forster, R. J. *Electrochem. Commun.* **2014**, *48*, 95.

DOI: 10.1021/jacs.6b03662
J. Am. Chem. Soc. 2016, 138, 7718−7724